

WMamba: Wavelet-based Mamba for Face Forgery Detection

Siran Peng^{1,2}, Tianshuo Zhang^{2,1}, Li Gao³, Xiangyu Zhu^{1,2}, Haoyuan Zhang^{2,1}, Kai Pang⁴ and Zhen Lei^{1,2,5*}

¹MAIS, Institute of Automation, Chinese Academy of Sciences

²School of Artificial Intelligence, University of Chinese Academy of Sciences

³China Mobile Communications Company Limited Research Institute

⁴Guangzhou Pixel Solutions Co., Ltd.

⁵CAIR, HKISI, Chinese Academy of Sciences

{pengsiran2023, xiangyu.zhu, zhanghaoyuan2023, zhen.lei}@ia.ac.cn, tianshuo.zhang@nlpr.ia.ac.cn, gaolids@chinamobile.com, pangkai@pixelall.com

Abstract

With the rapid advancement of deepfake generation technologies, the demand for robust and accurate face forgery detection algorithms has become increasingly critical. Recent studies have demonstrated that wavelet analysis can uncover subtle forgery artifacts that remain imperceptible in the spatial domain. Wavelets effectively capture important facial contours, which are often slender, fine-grained, and global in nature. However, existing wavelet-based approaches fail to fully leverage these unique characteristics, resulting in sub-optimal feature extraction and limited generalizability. To address this challenge, we introduce WMamba, a novel wavelet-based feature extractor built upon the Mamba architecture. WMamba maximizes the utility of wavelet information through two key innovations. First, we propose Dynamic Contour Convolution (DCCConv), which employs specially crafted deformable kernels to adaptively model slender facial contours. Second, by leveraging the Mamba architecture, our method captures long-range spatial relationships with linear computational complexity. This efficiency allows for the extraction of fine-grained, global forgery artifacts from small image patches. Extensive experimental results show that WMamba achieves state-of-the-art (SOTA) performance, highlighting its effectiveness and superiority in face forgery detection.

1 Introduction

Recent advancements in deepfake generation technologies [Nirkin *et al.*, 2019; Li *et al.*, 2019] have garnered significant attention due to their ability to produce highly realistic digital faces that are often indistinguishable from real human appearances. While these technologies offer entertainment value, their potential for misuse, such as facilitating fraud, spreading misinformation, and fabricating fake news, poses serious

*Corresponding author

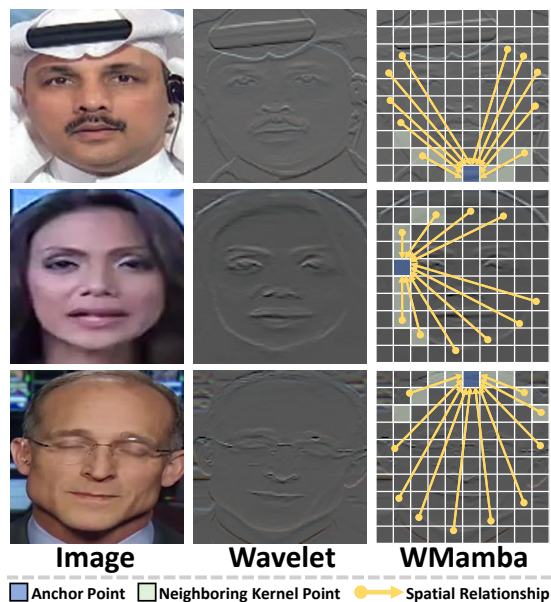


Figure 1: **Column 1:** Example frames from the FaceForensics++ (FF++) dataset. **Column 2:** Wavelets capture facial contours that are slender, fine-grained, and global in nature. **Column 3:** WMamba maximizes the potential of wavelet information via two innovations: DCCConv for precise modeling of slender facial contours (see the green squares) and Mamba for extracting fine-grained and global forgery artifacts from small image patches (see the yellow arrows).

social risks. As a result, there is an urgent need to develop robust and accurate algorithms for detecting face forgeries.

Detecting facial forgery artifacts directly in the spatial domain is challenging. Consequently, many approaches leverage frequency analysis techniques to reveal subtle manipulation traces that are imperceptible in spatial representations [Qian *et al.*, 2020; Li *et al.*, 2021]. Among these techniques, wavelet analysis has gained significant attention due to its ability to capture intricate frequency components while preserving essential spatial characteristics [Jia *et al.*, 2021; Liu *et al.*, 2022a; Li *et al.*, 2022; Miao *et al.*, 2023]. Specifically, wavelets capture key facial contours that are typically

slender (long and narrow), fine-grained (usually one to two pixels wide), and global (spanning extensive regions of the entire image), as illustrated in Figure 1. These contours often encode subtle yet valuable forgery clues, making them crucial for detecting manipulations. However, existing wavelet-based approaches primarily use conventional convolutions or Transformers for feature extraction, which limits their ability to fully exploit the complex characteristics of wavelet data.

To tackle this challenge, we introduce WMamba, a novel wavelet-based feature extractor built upon the Mamba architecture. WMamba fully considers the slender, fine-grained, and global characteristics of facial contours, maximizing the potential of wavelet information through two critical innovations. First, motivated by previous studies on deformable convolution [Dai *et al.*, 2017; Qi *et al.*, 2023], we present Dynamic Contour Convolution (DCCConv), which utilizes meticulously crafted deformable kernels to adaptively capture the slender structures of facial contours. Second, our method leverages the Mamba architecture [Gu and Dao, 2023], a highly effective alternative to traditional Convolutional Neural Networks (CNNs) and Transformers. Rooted in the State Space Model (SSM), Mamba excels at capturing long-range relationships while maintaining linear computational complexity with respect to the number of input tokens. This efficiency facilitates the use of smaller image patches, enabling the extraction of fine-grained and global forgery artifacts. In conclusion, the **contributions** of this paper are as follows:

1. We propose Dynamic Contour Convolution (DCCConv), an innovative variant of deformable convolution that utilizes carefully designed deformable kernels to adaptively capture the slender structures of facial contours.
2. We demonstrate the effectiveness of Mamba in detecting face forgeries. Mamba excels at capturing long-range dependencies while maintaining linear computational complexity, which allows it to extract fine-grained and global facial forgery clues from small image patches.
3. By combining DCCConv with Mamba, the proposed WMamba fully leverages the power of wavelet information. Extensive experimental results show that WMamba achieves state-of-the-art (SOTA) performance in both cross-dataset and cross-manipulation evaluations, underscoring its superiority in face forgery detection.

2 Related Works

2.1 Face Forgery Detection

Face forgery detection is typically framed as a binary classification problem, where the model takes an image or video as input and classifies it as either “real” or “fake”. Based on the strategies employed, existing detection methods can be broadly categorized into four main types: spatial-domain, frequency-domain, time-domain, and data-driven approaches. Spatial-domain methods detect face forgeries by examining variations in spatial details at the image level, such as color [He *et al.*, 2019], saturation [McCloskey and Albright, 2019], and artifacts [Shiohara and Yamasaki, 2022]. In contrast, time-domain methods analyze inter-frame inconsistencies, leveraging the entire video as input to identify ma-

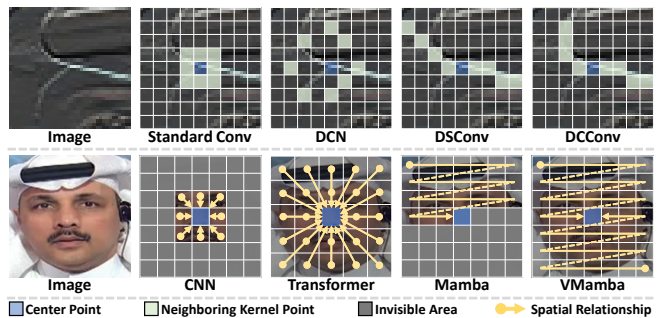


Figure 2: **Row 1:** Graphical illustration of Section 2.2, comparing various convolutional paradigms in their ability to capture slender structures. **Row 2:** Graphical illustration of Section 2.3, comparing the global perception capability across different methods. For clarity, only two flattening directions of VMamba are visualized.

nipulations [Yang *et al.*, 2023; Peng *et al.*, 2024]. Frequency-domain methods convert spatial- or time-domain data into the frequency domain using algorithms such as Discrete Cosine Transform (DCT) and Discrete Wavelet Transform (DWT) [Qian *et al.*, 2020; Tan *et al.*, 2024]. These techniques are particularly effective in uncovering subtle forgery traces that are imperceptible in the spatial or time domain. Finally, data-driven methods focus on optimizing model architectures and training strategies to fully exploit the potential of available data [Zhao *et al.*, 2021]. Based on the above categorizations, WMamba can be identified as a frequency-domain method.

2.2 Deformable Convolution

Standard convolution operations rely on fixed geometric patterns in their kernels, hindering their adaptability to objects exhibiting diverse shapes and orientations. To address this limitation, the Deformable Convolutional Network (DCN) [Dai *et al.*, 2017] introduces learnable offsets that dynamically adjust the kernel’s shape, allowing for better alignment with the target’s geometry. While this innovation empowers networks to model diverse geometric structures, DCN still faces challenges when dealing with slender shapes. To overcome this shortcoming, the Dynamic Snake Convolution (DSConv) [Qi *et al.*, 2023] was proposed. DSConv simulates slender structures by imposing constraints on both the kernel shape and the offset learning process. In 2D, for instance, it initializes with a 1D kernel oriented along a fixed coordinate axis (x or y). The kernel samples form an equidistant sequence along this primary axis. DSConv then iteratively calculates the perpendicular offsets for each sample point, with a key constraint: the offset difference between neighboring points cannot exceed one. This design enables the representation of slender shapes with smooth and continuous topologies. However, the dependence on a predefined axis restricts DSConv’s ability to capture structures that orient in other directions, significantly reducing its flexibility. These convolutional paradigms are visually illustrated in Row 1 of Figure 2.

2.3 Mamba

Most deep learning-based computer vision methods rely on CNNs or Transformers for feature extraction. While CNNs

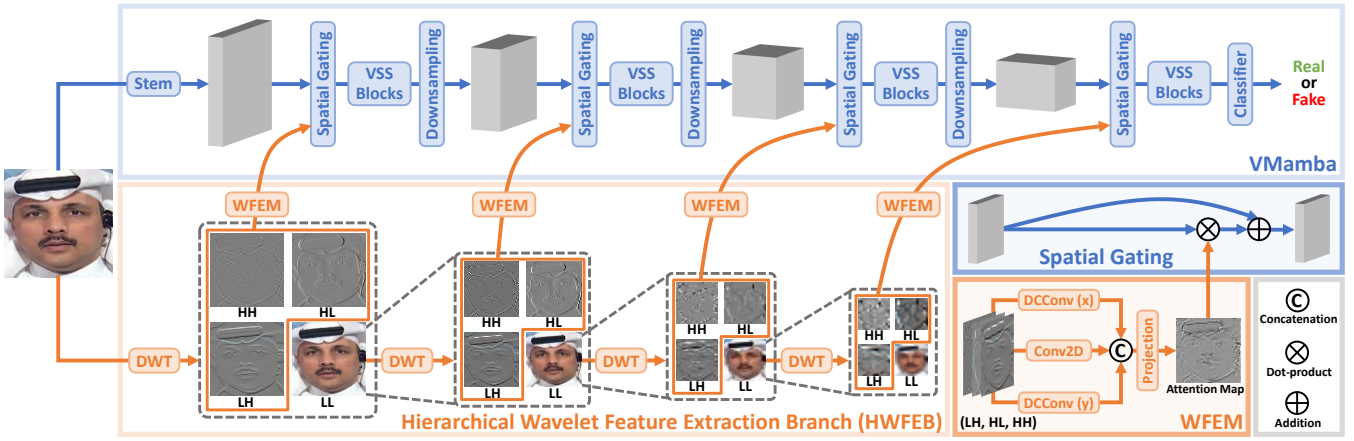


Figure 3: Overview of WMamba. The proposed architecture consists of two primary components: the HWFEB and the VMamba model. The HWFEB utilizes a multi-level DWT to generate wavelet representations at various scales and leverages WFEMs to produce spatial attention maps from these representations. VMamba extracts wavelet-enhanced facial forgery clues and outputs the final classification result.

are efficient, their limited receptive fields hinder their ability to capture global context. In contrast, Transformers excel at modeling long-range relationships but suffer from quadratic computational complexity. To mitigate this, Transformer-based methods typically segment input images into large patches, which may cause a loss of fine-grained spatial details. Recently, the Mamba architecture [Gu and Dao, 2023], based on the SSM, has emerged as a promising alternative by achieving global perception with linear complexity. However, Mamba was initially designed for 1D tasks with inherent directional structures. Directly extending it to 2D vision tasks, where such directional patterns are often absent, can lead to incomplete global perception. To tackle this challenge, Vision Mamba [Zhu *et al.*, 2024] introduces a bidirectional flattening approach that flattens spatial feature maps along both positive and negative directions, resulting in a more comprehensive global perception. Building on this, VMamba [Liu *et al.*, 2024] proposes a four-directional flattening technique, enabling the discovery of richer spatial relationships. These methods are visually illustrated in Row 2 of Figure 2.

3 Methodology

3.1 Overview

The proposed WMamba network architecture consists of two primary components: a Hierarchical Wavelet Feature Extraction Branch (HWFEB) and a VMamba model, as illustrated in Figure 3. Given an input RGB image, the HWFEB begins by applying a multi-level DWT to generate wavelet representations across various scales. Subsequently, these representations are processed by Wavelet Feature Extraction Modules (WFEMs), which primarily leverage DCCConv to produce spatial attention maps. Next, these attention maps are seamlessly integrated into the VMamba model through spatial gating mechanisms. Finally, the model outputs two probabilities, classifying the input image as either real or fake. Since this paper concentrates on network architecture, we adopt the standard Cross-Entropy (CE) Loss as the loss function for

training. The remainder of this section is organized as follows: Section 3.2 describes the WMamba pipeline in detail, and Section 3.3 provides an in-depth explanation of DCCConv.

3.2 WMamba

In this section, we provide a detailed description of the two key components of WMamba: the HWFEB and VMamba.

HWFEB. We begin by utilizing a multi-level Haar DWT to generate wavelet representations at different scales. For an input image $I \in \mathbb{R}^{H \times W \times 3}$, where H and W denote the height and width, the Haar DWT operates by convolving I with four distinct filters: f_{LL} , f_{LH} , f_{HL} , and f_{HH} . These filters correspond to the Low-Low, Low-High, High-Low, and High-High frequency sub-bands, producing the respective wavelet sub-band outputs: LL, LH, HL, and HH, each of size $\frac{H}{2} \times \frac{W}{2} \times 3$. This process can be mathematically expressed as follows:

$$\begin{aligned}
 LL, LH, HL, HH &= (f_{LL}, f_{LH}, f_{HL}, f_{HH}) \otimes I, \\
 f_{LL}, f_{LH}, f_{HL}, f_{HH} &= \begin{bmatrix} \frac{1}{2} & \frac{1}{2} \\ \frac{1}{2} & \frac{1}{2} \end{bmatrix}, \begin{bmatrix} \frac{1}{2} & \frac{1}{2} \\ -\frac{1}{2} & -\frac{1}{2} \end{bmatrix}, \begin{bmatrix} \frac{1}{2} & -\frac{1}{2} \\ \frac{1}{2} & -\frac{1}{2} \end{bmatrix}, \begin{bmatrix} \frac{1}{2} & -\frac{1}{2} \\ -\frac{1}{2} & \frac{1}{2} \end{bmatrix}.
 \end{aligned} \tag{1}$$

Here, \otimes represents the convolution operation. The LH, HL, and HH sub-bands preserve high-frequency details, such as edges and textures, across different orientations. In contrast, the LL sub-band essentially serves as a low-resolution version of the input image and can be recursively decomposed. This recursive process forms a multi-level DWT, which enables the generation of wavelet representations across various scales.

Subsequently, we leverage WFEMs to generate spatial attention maps from the wavelet sub-bands LH, HL, and HH across multiple scales. This involves extracting forgery features using a combination of three parallel convolutional layers: two DCCConv layers (one initialized along the x-axis and the other along the y-axis) and one standard 2D convolutional layer. The DCCConv layers specialize in capturing the slender structures of facial contours, while the standard convolutional layer focuses on learning broader, more generalized patterns. The resulting feature maps from these layers are concatenated

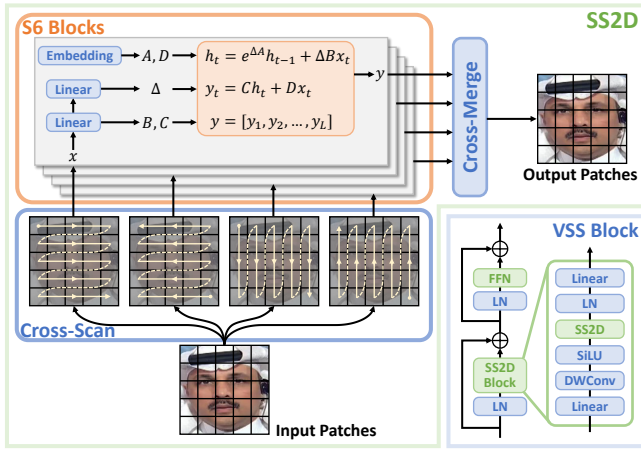


Figure 4: Schematic diagram of the VSS block. At its core lies the SS2D mechanism, which flattens input image patches along four principle directions to facilitate comprehensive global perception. Additionally, the variable L represents the number of patches.

and projected to create the desired spatial attention map.

Next, we integrate spatial attention maps into the VMamba model using spatial gating mechanisms. Specifically, the attention map is applied to the model’s feature map via a dot-product operation, which spatially weights the features to emphasize critical forgery clues. In addition, a skip connection is employed to enhance the model’s stability and convergence. **VMamba.** The Mamba architecture is based on the SSM, a foundational framework widely used in control theory and signal processing. The SSM maps a 1D input signal $x(t) \in \mathbb{R}$ to an output signal $y(t) \in \mathbb{R}$ through the continuous-time evolution of hidden states $h(t) \in \mathbb{R}^N$, where N represents the state dimension. This dynamic system is defined by the following set of Ordinary Differential Equations (ODEs):

$$\begin{aligned} h'(t) &= Ah(t) + Bx(t), \\ y(t) &= Ch(t) + Dx(t). \end{aligned} \quad (2)$$

Here, $A \in \mathbb{R}^{N \times N}$ is the state matrix governing the system’s temporal evolution. $B \in \mathbb{R}^{N \times 1}$, $C \in \mathbb{R}^{1 \times N}$, and $D \in \mathbb{R}^{1 \times 1}$ are input, output, and feedthrough projection parameters, respectively. The system exhibits global memory characteristics, as evidenced by Equation 2, where each output depends on the entire history of past inputs through recursive state propagation. When implementing the SSM in deep learning applications, discretization is essential to transform the continuous-time system into its discrete-time equivalent. This process introduces a timescale parameter $\Delta \in \mathbb{R}$ that maps the continuous parameters A and B to their discrete counterparts \bar{A} and \bar{B} . Using the Zero-Order Hold (ZOH) algorithm, the discrete parameters are computed as follows:

$$\begin{aligned} \bar{A} &= e^{\Delta A}, \\ \bar{B} &= (\Delta A)^{-1}(e^{\Delta A} - E) \cdot \Delta B \approx \Delta B. \end{aligned} \quad (3)$$

Here, $E \in \mathbb{R}^{N \times N}$ denotes the identity matrix. Then, the discrete form of Equation 2 can be written as follows:

$$\begin{aligned} h_t &= \bar{A}h_{t-1} + \bar{B}x_t, \\ y_t &= Ch_t + Dx_t. \end{aligned} \quad (4)$$

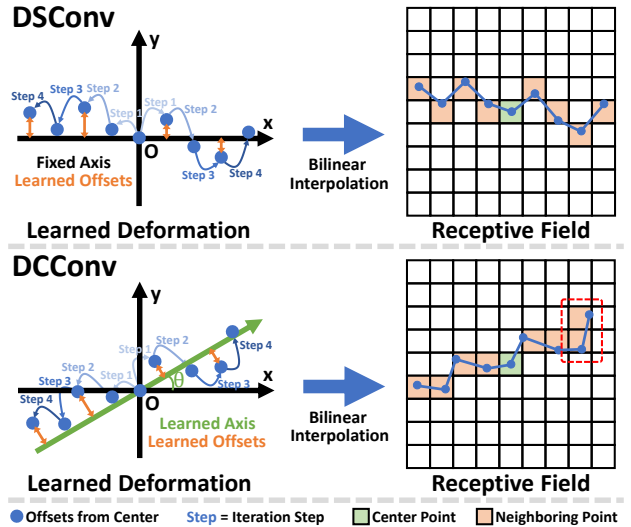


Figure 5: Schematic diagram of DSConv and the proposed DCCConv (initialized along the x-axis). DSConv learns perpendicular offsets to model slender structures oriented along a fixed direction. In contrast, DCCConv predicts both offsets and axis orientation, allowing it to represent slender structures aligned in any direction. Notably, the shape highlighted in the red box is unachievable with DSConv.

In practice, x_t is a feature vector with C components, and each of which is processed independently through Equation 4.

The VMamba model, a 2D adaptation of Mamba, utilizes hierarchical Visual State Space (VSS) blocks to extract rich forgery signatures from image patches at multiple spatial resolutions. As illustrated in Figure 4, each VSS block consists of two key components: a Selective-Scan 2D (SS2D) block and a Feed Forward Network (FFN). The SS2D block performs channel projection operations and employs an SS2D mechanism to capture fine-grained and global facial forgery artifacts from the input image patches. Following this, the FFN extracts channel-specific facial features, further enhancing the model’s ability to learn and identify forgery artifacts.

The SS2D mechanism is composed of three components: a cross-scan module, a stack of four S6 blocks, and a cross-merge module. The cross-scan module scans input image patches along four principal directions (horizontal, vertical, and both diagonals), creating flattened sequences that capture multi-directional spatial relationships. At the heart of the SS2D is the S6 block, a pivotal innovation introduced by Mamba, which integrates a selective-scan mechanism to enhance Equation 4. This mechanism dynamically learns projection and timescale parameters from the input data, boosting the model’s flexibility and expressiveness. Finally, the cross-merge module reconstructs the original spatial structure by unflattening the processed sequences and merging them into a cohesive output image through fusion operations.

3.3 DCCConv

Building upon DSConv, we propose DCCConv, which incorporates a learned coordinate axis to effectively capture a wider variety of slender structures. A detailed comparison of the two algorithms is presented in Figure 5. Specifically, we start

Method	Input Type	Training Set		Test Set AUC (%)			
		Real	Fake	CDF	DFDC	DFDCP	FFIW
F ³ -Net* [Qian <i>et al.</i> , 2020]	Frame	✓	✓	77.92	67.35	73.54	70.11
LTW* [Sun <i>et al.</i> , 2021]	Frame	✓	✓	77.14	69.00	74.58	76.63
PCL+I2G [Zhao <i>et al.</i> , 2021]	Frame	✓		90.03	67.52	74.37	-
DCL [Sun <i>et al.</i> , 2022]	Frame	✓	✓	82.30	76.71	-	-
SBI [Shiohara and Yamasaki, 2022]	Frame	✓		93.18	72.42	86.15	<u>84.83</u>
F ² Trans [Miao <i>et al.</i> , 2023]	Frame	✓	✓	89.87	76.15	-	-
SeeABLE [Larue <i>et al.</i> , 2023]	Frame	✓		87.30	75.90	86.30	-
AUNet [Bai <i>et al.</i> , 2023]	Frame	✓		92.77	73.82	86.16	81.45
MoE-FFD [Kong <i>et al.</i> , 2024]	Frame	✓	✓	91.28	-	84.97	-
LAA-Net [Nguyen <i>et al.</i> , 2024]	Frame	✓		95.40	-	86.94	-
RAE [Tian <i>et al.</i> , 2024]	Frame	✓		<u>95.50</u>	<u>80.20</u>	<u>89.50</u>	-
FTCN* [Zheng <i>et al.</i> , 2021]	Video	✓	✓	86.90	71.00	74.00	74.47
RealForensics [Haliassos <i>et al.</i> , 2022]	Video	✓	✓	86.90	75.90	-	-
TALL [Xu <i>et al.</i> , 2023]	Video	✓	✓	90.79	76.78	-	-
TALL++ [Xu <i>et al.</i> , 2024]	Video	✓	✓	91.96	78.51	-	-
NACO [Zhang <i>et al.</i> , 2024]	Video	✓	✓	89.50	76.70	-	-
WMamba (Ours)	Frame	✓		96.29	82.97	89.62	86.59

Table 1: Cross-dataset evaluation of face forgery detection methods on the CDF, DFDC, DFDCP, and FFIW datasets. Methods marked with the symbol * are reproduced using the official codes, while results for other methods are cited directly from their respective papers. The best performance is highlighted in **bold**, and the second best is underlined. Notably, WMamba achieves SOTA performance across all datasets.

with a 1D convolutional kernel that is oriented along a pre-defined coordinate axis (either the x-axis or y-axis). For a given input feature map, DCCConv employs a standard 2D convolutional layer to dynamically generate pixel-wise offsets and rotation angles. The predicted offsets are constrained within the interval $[-1, 1]$ using a Tanh activation function, while the rotation angles are restricted to the range $[0, \frac{\pi}{2}]$ through a Sigmoid activation function. Let the positions of the 1D kernel, centered at the i -th pixel (x_i, y_i) , be denoted as $\{K_{i\pm c} = (x_{i\pm c}, y_{i\pm c}) \mid c = 0, 1, \dots, \frac{k-1}{2}\}$, where k represents the kernel length. The corresponding learned offsets and rotation angles are given by $\{\delta_{i,\pm c} \mid c = 0, 1, \dots, \frac{k-1}{2}\}$ and θ_i , respectively. When the 1D kernel is oriented along the x-axis, the adjusted positions of the kernel can be iteratively calculated using the following equation:

$$K_{i\pm c} = (x_i, y_i) + (\pm c, \sum_{j=0}^c \delta_{i,\pm j}) \cdot \begin{bmatrix} \cos \theta_i & -\sin \theta_i \\ \sin \theta_i & \cos \theta_i \end{bmatrix}. \quad (5)$$

Notably, in practice, $\delta_{i,0}$ is set to 0. When the 1D kernel is aligned with the y-axis, Equation 5 can be rewritten as:

$$K_{i\pm c} = (x_i, y_i) + (\sum_{j=0}^c \delta_{i,\pm j}, \pm c) \cdot \begin{bmatrix} \cos \theta_i & -\sin \theta_i \\ \sin \theta_i & \cos \theta_i \end{bmatrix}. \quad (6)$$

The Tanh activation function and the iterative calculation process ensure that the offset differences between adjacent kernel points remain below one. This allows for the effective extraction of slender structures with smooth and continuous topologies. Moreover, the learned rotation angles enable DCCConv to theoretically model slender structures oriented in any

direction. Given that the offsets are typically fractional, bilinear interpolation is employed to compute the receptive field values for the convolution operation [Dai *et al.*, 2017].

4 Experiments

4.1 Setup

Datasets. For training, we utilize the widely adopted FaceForensics++ (FF++) [Rossler *et al.*, 2019] benchmark dataset, which comprises 1,000 authentic face videos and 4,000 manipulated videos generated using four distinct forgery techniques: DeepFakes (DF), Face2Face (F2F) [Thies *et al.*, 2016], FaceSwap (FS), and NeuralTextures (NT) [Thies *et al.*, 2019]. Notably, our approach utilizes the SBI algorithm [Shiohara and Yamasaki, 2022], which exclusively trains on real face videos, enabling the cross-manipulation evaluation across all four forgery types in FF++. To evaluate cross-dataset generalization capabilities, we test our network on four prominent datasets: Celeb-DeepFake-v2 (CDF) [Li *et al.*, 2020], which employs advanced deepfake methods on YouTube celebrity content; DeepFake Detection Challenge (DFDC) [Dolhansky *et al.*, 2020] and its Preview version (DFDCP) [Dolhansky, 2019], which feature videos with various perturbations including compression, downsampling, and noise; and FFIW-10K (FFIW) [Zhou *et al.*, 2021], which introduces additional complexity via multi-person scenarios.

Frame-Level Baselines. We evaluate our approach against eleven SOTA frame-level baselines for face forgery detection. These methods employ diverse strategies: F³-Net [Qian *et al.*, 2020] leverages frequency-aware manipulation clues, LTW [Sun *et al.*, 2021] focuses on domain-general detection,

Method	Test Set AUC (%)				
	DF	F2F	FS	NT	FF++
PCL+I2G	100	98.97	99.86	97.63	99.11
SBI	<u>99.99</u>	<u>99.88</u>	<u>99.91</u>	<u>98.79</u>	<u>99.64</u>
SeeABLE	99.20	98.80	99.10	96.90	98.50
AUNet	99.98	99.60	99.89	98.38	99.46
RAE	99.60	99.10	99.20	97.60	98.90
WMamba	100	99.98	99.94	98.88	99.70

Table 2: Cross-manipulation evaluation of methods trained exclusively on real face videos from FF++. Notably, our method consistently delivers the best results across all tested manipulations.

PCL+I2G [Zhao *et al.*, 2021] analyzes source feature inconsistencies, DCL [Sun *et al.*, 2022] implements multi-granular contrastive learning, and SBI [Shiohara and Yamasaki, 2022] generates synthetic fake faces for training purposes. Additionally, F²-Trans [Miao *et al.*, 2023] combines spatial and frequency domain forgery traces, SeeABLE [Larue *et al.*, 2023] reformulates face forgery detection as an Out-Of-Distribution (OOD) problem, AUNet [Bai *et al.*, 2023] investigates facial Action Unit (AU) regions, MoE-FFD [Kong *et al.*, 2024] incorporates Mixture-of-Experts (MoE) modules, LAA-Net [Nguyen *et al.*, 2024] utilizes heatmap-guided self-consistency attention, and RAE [Tian *et al.*, 2024] learns to recover real facial appearances from perturbations.

Video-Level Baselines. We further compare our method with five video-level face forgery detection approaches. These include FTCN [Zheng *et al.*, 2021], which exploits temporal coherence patterns; RealForensics [Haliassos *et al.*, 2022], which employs a two-stage detection framework trained on natural talking face datasets; TALL [Xu *et al.*, 2023], which preserves spatio-temporal dependencies through layout transformation; its enhanced version TALL++ [Xu *et al.*, 2024], which incorporates the Graph Reasoning Block (GRB) and Semantic Consistency (SC) loss; and NACO [Zhang *et al.*, 2024], which learns natural consistency representations from real face videos for improved generalization and robustness.

Evaluation Metric. We evaluate detection performance using the Area Under the Receiver Operating Characteristic Curve (AUC), a standard metric in face forgery detection. For frame-level methods, we report video-level results, which average the predictions across all frames within each video, allowing for a direct comparison with video-level approaches.

Implementation Details. Our implementation adopts the preprocessing pipeline and data augmentation strategy outlined in SBI [Shiohara and Yamasaki, 2022], along with their synthetic data generation methodology. For further information, please refer to the supplementary materials. We employ VMamba-S [Liu *et al.*, 2024] as the backbone network, which is pre-trained on ImageNet-1K [Deng *et al.*, 2009]. Additionally, we configure DCCConv with a kernel length of 9. The WMamba model is trained using the AdamW optimizer with a batch size of 32, an initial learning rate of 5e-5, and a total of 200 epochs. To improve convergence, the learning rate is linearly decayed starting from the 100th epoch, allowing for a smooth adjustment over the remaining training period. Imple-

Method	Test Set AUC (%)			
	CDF	DFDC	DFDCP	FFIW
w/ LL	<u>95.61</u>	80.25	87.47	85.68
w/o Hierarchical	94.76	<u>81.79</u>	<u>87.88</u>	85.03
w/ Addition	94.70	77.57	87.13	<u>86.34</u>
w/ Concatenation	84.54	69.19	78.22	65.05
w/o Skip Connection	95.14	78.51	85.75	84.61
The Proposed	96.29	82.97	89.62	86.59

Table 3: Ablation study results on the structural design of HWFEB.

Method	Test Set AUC (%)			
	CDF	DFDC	DFDCP	FFIW
w/ DCN	95.15	80.15	<u>87.77</u>	85.53
w/ DSConv	94.42	<u>82.87</u>	85.83	<u>86.26</u>
w/o DCCConv	<u>96.06</u>	80.24	87.21	85.88
The Proposed	96.29	82.97	89.62	86.59

Table 4: Ablation study results for the proposed DCCConv.

mented in the PyTorch environment, training WMamba with these settings requires approximately 30GB of GPU memory.

4.2 Results

Cross-Dataset Evaluation. The cross-dataset evaluation is a key testing protocol for face forgery detection, as it assesses a method’s ability to generalize to unseen data. We compare our method with recent SOTA approaches and present the results in Table 1. The proposed WMamba achieves the highest AUC scores across all unseen datasets, demonstrating its exceptional generalization capability. This outstanding performance can be attributed to the effectiveness of DCCConv and VMamba, which harness the full potential of wavelet information, enabling comprehensive extraction of forgery clues.

Cross-Manipulation Evaluation. In practice, defenders are often unaware of the specific forgery techniques used by attackers. Consequently, it is crucial to assess a model’s ability to generalize across various types of manipulations. Following the protocol in [Shiohara and Yamasaki, 2022], we compare our method with approaches trained solely on real face videos from FF++. The results, shown in Table 2, highlight WMamba’s effectiveness in handling unseen manipulations.

4.3 Ablation Studies

In this section, we present the results of our ablation studies on HWFEB, DCCConv, and VMamba. Additional ablation study findings are provided in the supplementary materials.

Structural Analysis of the HWFEB. We validate the design choices of HWFEB through comprehensive ablation studies conducted on five architectural variants. Specifically, our experiments investigate: (1) the impact of including the LL component in WFEMs (w/ LL), compared to our baseline using only LH, HL, and HH sub-bands for wavelet guidance; (2) the benefits of employing multi-scale wavelet representations over single-scale analysis (w/o Hierarchical); and (3) the effectiveness of the spatial gating mechanism versus alternative

Backbone	Params	Test Set AUC (%)			
		CDF	DFDC	DFDCP	FFIW
VMamba-T	30M	<u>95.82</u>	<u>82.00</u>	<u>88.03</u>	83.15
VMamba-S	50M	96.29	82.97	89.62	<u>86.59</u>
VMamba-B	89M	95.29	81.64	88.09	87.29

Table 5: Comparison of different VMamba backbone versions.

Method	Test Set AUC (%)			
	CDF	DFDC	DFDCP	FFIW
ConvNeXt-S	94.39	80.23	86.26	82.04
ConvNeXt-S+HWFEB	94.46	<u>82.17</u>	86.22	84.60
ViT-B16	93.64	79.66	85.73	83.92
Swin-S	95.26	80.06	86.80	84.87
Swin-S+HWFEB	<u>95.60</u>	81.01	<u>87.91</u>	<u>86.33</u>
VMamba-S	95.39	81.37	86.93	85.60
VMamba-S+HWFEB	96.29	82.97	89.62	86.59

Table 6: Comparison of different network architectures. Both ConvNeXt-S and Swin-S have 50M parameters, whereas ViT-B16 has a higher parameter count of 87M. Notably, ViT-B16 extracts features at a single scale, which makes it incompatible with HWFEB.

feature fusion strategies (w/ Addition, w/ Concatenation, and w/o Skip Connection). The cross-dataset evaluation results, presented in Table 2, validate our design decisions by demonstrating superior performance across all tested variants.

Effectiveness of DCCConv. To validate the efficacy of our proposed DCCConv, we conduct comparative experiments against DCN [Dai *et al.*, 2017], DSConv [Qi *et al.*, 2023], and a baseline network without DCCConv. The cross-dataset evaluation results, shown in Table 4, demonstrate that DCCConv consistently outperforms existing approaches, highlighting its superior ability to capture the slender structures of facial contours.

Analysis of VMamba. We begin with a systematic evaluation of the three VMamba backbone versions: VMamba-T (Tiny), VMamba-S (Small), and VMamba-B (Base). The cross-dataset assessment results, presented in Table 5, challenge the conventional assumption that larger architectures inherently deliver better performance. Notably, VMamba-S outperforms both its smaller and larger counterparts, which led to its selection as the backbone network for WMamba.

Next, our investigation explores the relationship between patch count and model performance by systematically varying the input image sizes. The cross-dataset evaluation results in Figure 6 reveal that, in general, model performance improves with an increase in the number of patches. The peak performance is observed at a patch count of 3136, which corresponds to an input size of 224×224 pixels, the same resolution used during the pretraining of the VMamba-S backbone.

Finally, we compare VMamba against three widely used network architectures: the CNN-based ConvNeXt [Liu *et al.*, 2022b], and the Transformer-based ViT [Dosovitskiy *et al.*, 2021] and Swin [Liu *et al.*, 2021]. ViT processes features at a fixed 14×14 spatial resolution, whereas other architec-

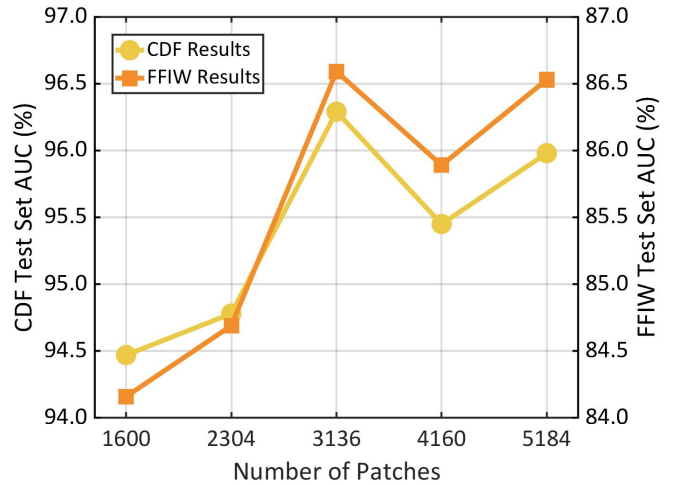


Figure 6: Impact of patch count on model performance. The horizontal axis shows the number of patches following the Stem module in the VMamba model. Overall, performance improves with an increase in patch count. Notably, the peak performance is observed at a patch count of 3136, which corresponds to the configuration utilized during the pretraining of the VMamba-S backbone.

tures adopt a hierarchical design, extracting features across multiple scales (up to 56×56). Adapting ViT to support multi-scale feature extraction would drastically increase its computational cost by approximately two orders of magnitude, making it impractical for this task. Although Swin improves efficiency through windowed attention, this localized approach inherently limits its ability to effectively capture long-range spatial relationships. To ensure a fair comparison, all compared backbones are pre-trained on ImageNet-1K and matched in terms of parameter count. The cross-dataset evaluation results, presented in Table 6, reveal two significant findings: (1) VMamba outperforms CNN- and Transformer-based architectures, highlighting its superior capability in face forgery detection; and (2) incorporating the HWFEB consistently enhances detection performance, demonstrating its versatility and effectiveness as a plug-and-play module.

5 Conclusion

In this paper, we introduce WMamba, a wavelet-based feature extractor built upon the Mamba architecture. WMamba fully considers the slender, fine-grained, and global characteristics of facial contours, maximizing the utility of wavelet information through two key innovations. First, inspired by DSConv, we propose DCCConv, which captures a broader range of slender structures by learning an adaptive coordinate axis. Second, by leveraging the Mamba architecture, which excels at capturing long-range spatial dependencies with linear complexity, our method effectively extracts fine-grained and global forgery clues from small patches. The proposed WMamba achieves SOTA performance in both cross-dataset and cross-manipulation evaluations, demonstrating its effectiveness in detecting face forgeries. Furthermore, extensive ablation studies confirm the validity of our network design, highlighting the unique contributions of each component.

References

- [Bai *et al.*, 2023] Weiming Bai, Yufan Liu, Zhipeng Zhang, Bing Li, and Weiming Hu. Aunet: Learning relations between action units for face forgery detection. In *Proceedings of the IEEE/CVF Conference on Computer Vision and Pattern Recognition (CVPR)*, pages 24709–24719, 2023.
- [Dai *et al.*, 2017] Jifeng Dai, Haozhi Qi, Yuwen Xiong, Yi Li, Guodong Zhang, Han Hu, and Yichen Wei. Deformable convolutional networks. In *Proceedings of the IEEE International Conference on Computer Vision (ICCV)*, 2017.
- [Deng *et al.*, 2009] Jia Deng, Wei Dong, Richard Socher, Li-Jia Li, Kai Li, and Li Fei-Fei. Imagenet: A large-scale hierarchical image database. In *2009 IEEE Conference on Computer Vision and Pattern Recognition (CVPR)*, pages 248–255, 2009.
- [Dolhansky *et al.*, 2020] Brian Dolhansky, Joanna Bitton, Ben Pflaum, Jikuo Lu, Russ Howes, Menglin Wang, and Cristian Canton Ferrer. The deepfake detection challenge (dfdc) dataset. *arXiv preprint arXiv:2006.07397*, 2020.
- [Dolhansky, 2019] B Dolhansky. The dee pfake detection challenge (dfdc) pre view dataset. *arXiv preprint arXiv:1910.08854*, 2019.
- [Dosovitskiy *et al.*, 2021] Alexey Dosovitskiy, Lucas Beyer, Alexander Kolesnikov, Dirk Weissenborn, Xiaohua Zhai, Thomas Unterthiner, Mostafa Dehghani, Matthias Minderer, Georg Heigold, Sylvain Gelly, Jakob Uszkoreit, and Neil Houlsby. An image is worth 16x16 words: Transformers for image recognition at scale. In *International Conference on Learning Representation (ICLR)*, 2021.
- [Gu and Dao, 2023] Albert Gu and Tri Dao. Mamba: Linear-time sequence modeling with selective state spaces. *arXiv preprint arXiv:2312.00752*, 2023.
- [Haliassos *et al.*, 2022] Alexandros Haliassos, Rodrigo Mira, Stavros Petridis, and Maja Pantic. Leveraging real talking faces via self-supervision for robust forgery detection. In *Proceedings of the IEEE/CVF Conference on Computer Vision and Pattern Recognition (CVPR)*, pages 14950–14962, June 2022.
- [He *et al.*, 2019] Peisong He, Haoliang Li, and Hongxia Wang. Detection of fake images via the ensemble of deep representations from multi color spaces. In *2019 IEEE International Conference on Image Processing (ICIP)*, pages 2299–2303, 2019.
- [Jia *et al.*, 2021] Gengyun Jia, Meisong Zheng, Chuanrui Hu, Xin Ma, Yuting Xu, Luoqi Liu, Yafeng Deng, and Ran He. Inconsistency-aware wavelet dual-branch network for face forgery detection. *IEEE Transactions on Biometrics, Behavior, and Identity Science*, 3(3):308–319, 2021.
- [Kong *et al.*, 2024] Chenqi Kong, Anwei Luo, Peijun Bao, Yi Yu, Haoliang Li, Zengwei Zheng, Shiqi Wang, and Alex C Kot. Moe-ffd: Mixture of experts for generalized and parameter-efficient face forgery detection. *arXiv preprint arXiv:2404.08452*, 2024.
- [Larue *et al.*, 2023] Nicolas Larue, Ngoc-Son Vu, Vitomir Struc, Peter Peer, and Vassilis Christophides. Seeable: Soft discrepancies and bounded contrastive learning for exposing deepfakes. In *Proceedings of the IEEE/CVF International Conference on Computer Vision (ICCV)*, pages 21011–21021, October 2023.
- [Li *et al.*, 2019] Lingzhi Li, Jianmin Bao, Hao Yang, Dong Chen, and Fang Wen. Faceshifter: Towards high fidelity and occlusion aware face swapping. *arXiv preprint arXiv:1912.13457*, 2019.
- [Li *et al.*, 2020] Yuezun Li, Xin Yang, Pu Sun, Honggang Qi, and Siwei Lyu. Celeb-df: A large-scale challenging dataset for deepfake forensics. In *Proceedings of the IEEE/CVF Conference on Computer Vision and Pattern Recognition (CVPR)*, June 2020.
- [Li *et al.*, 2021] Jiaming Li, Hongtao Xie, Jiahong Li, Zhongyuan Wang, and Yongdong Zhang. Frequency-aware discriminative feature learning supervised by single-center loss for face forgery detection. In *Proceedings of the IEEE/CVF Conference on Computer Vision and Pattern Recognition (CVPR)*, pages 6458–6467, 2021.
- [Li *et al.*, 2022] Jiaming Li, Hongtao Xie, Lingyun Yu, and Yongdong Zhang. Wavelet-enhanced weakly supervised local feature learning for face forgery detection. In *Proceedings of the 30th ACM International Conference on Multimedia (ACM MM)*, page 1299–1308, 2022.
- [Liu *et al.*, 2021] Ze Liu, Yutong Lin, Yue Cao, Han Hu, Yixuan Wei, Zheng Zhang, Stephen Lin, and Baining Guo. Swin transformer: Hierarchical vision transformer using shifted windows. In *Proceedings of the IEEE/CVF International Conference on Computer Vision (ICCV)*, pages 10012–10022, 2021.
- [Liu *et al.*, 2022a] Jie Liu, Jingjing Wang, Peng Zhang, Chunmao Wang, Di Xie, and Shiliang Pu. Multi-scale wavelet transformer for face forgery detection. In *Proceedings of the Asian Conference on Computer Vision (ACCV)*, pages 1858–1874, 2022.
- [Liu *et al.*, 2022b] Zhuang Liu, Hanzi Mao, Chao-Yuan Wu, Christoph Feichtenhofer, Trevor Darrell, and Saining Xie. A convnet for the 2020s. In *Proceedings of the IEEE/CVF Conference on Computer Vision and Pattern Recognition (CVPR)*, pages 11976–11986, 2022.
- [Liu *et al.*, 2024] Yue Liu, Yunjie Tian, Yuzhong Zhao, Hongtian Yu, Lingxi Xie, Yaowei Wang, Qixiang Ye, and Yunfan Liu. Vmamba: Visual state space model. *arXiv preprint arXiv:2401.10166*, 2024.
- [McCloskey and Albright, 2019] Scott McCloskey and Michael Albright. Detecting gan-generated imagery using saturation cues. In *2019 IEEE International Conference on Image Processing (ICIP)*, pages 4584–4588, 2019.
- [Miao *et al.*, 2023] Changtao Miao, Zichang Tan, Qi Chu, Huan Liu, Honggang Hu, and Nenghai Yu. F2trans: High-frequency fine-grained transformer for face forgery detection. *IEEE Transactions on Information Forensics and Security*, 18:1039–1051, 2023.

- [Nguyen *et al.*, 2024] Dat Nguyen, Nesryne Mejri, Inder Pal Singh, Polina Kulshova, Marcella Astrid, Anis Kacem, Enjie Ghorbel, and Djamila Aouada. Laa-net: Localized artifact attention network for quality-agnostic and generalizable deepfake detection. In *Proceedings of the IEEE/CVF Conference on Computer Vision and Pattern Recognition (CVPR)*, pages 17395–17405, June 2024.
- [Nirkin *et al.*, 2019] Yuval Nirkin, Yosi Keller, and Tal Hassner. Fsgan: Subject agnostic face swapping and reenactment. In *Proceedings of the IEEE/CVF International Conference on Computer Vision (ICCV)*, pages 7184–7193, 2019.
- [Peng *et al.*, 2024] Chunlei Peng, Zimin Miao, Decheng Liu, Nannan Wang, Ruimin Hu, and Xinbo Gao. Where deepfakes gaze at? spatial–temporal gaze inconsistency analysis for video face forgery detection. *IEEE Transactions on Information Forensics and Security*, 19:4507–4517, 2024.
- [Qi *et al.*, 2023] Yaolei Qi, Yuting He, Xiaoming Qi, Yuan Zhang, and Guanyu Yang. Dynamic snake convolution based on topological geometric constraints for tubular structure segmentation. In *Proceedings of the IEEE/CVF International Conference on Computer Vision (ICCV)*, pages 6070–6079, 2023.
- [Qian *et al.*, 2020] Yuyang Qian, Guojun Yin, Lu Sheng, Zixuan Chen, and Jing Shao. Thinking in frequency: Face forgery detection by mining frequency-aware clues. In *European conference on computer vision (ECCV)*, pages 86–103. Springer, 2020.
- [Rossler *et al.*, 2019] Andreas Rossler, Davide Cozzolino, Luisa Verdoliva, Christian Riess, Justus Thies, and Matthias Niessner. Faceforensics++: Learning to detect manipulated facial images. In *Proceedings of the IEEE/CVF International Conference on Computer Vision (ICCV)*, October 2019.
- [Shiohara and Yamasaki, 2022] Kaede Shiohara and Toshiko Yamasaki. Detecting deepfakes with self-blended images. In *Proceedings of the IEEE/CVF Conference on Computer Vision and Pattern Recognition (CVPR)*, pages 18720–18729, 2022.
- [Sun *et al.*, 2021] Ke Sun, Hong Liu, Qixiang Ye, Yue Gao, Jianzhuang Liu, Ling Shao, and Rongrong Ji. Domain general face forgery detection by learning to weight. In *Proceedings of the AAAI conference on artificial intelligence (AAAI)*, volume 35, pages 2638–2646, 2021.
- [Sun *et al.*, 2022] Ke Sun, Taiping Yao, Shen Chen, Shouhong Ding, Jilin Li, and Rongrong Ji. Dual contrastive learning for general face forgery detection. In *Proceedings of the AAAI Conference on Artificial Intelligence (AAAI)*, volume 36, pages 2316–2324, 2022.
- [Tan *et al.*, 2024] Chuangchuang Tan, Yao Zhao, Shikui Wei, Guanghua Gu, Ping Liu, and Yunchao Wei. Frequency-aware deepfake detection: Improving generalizability through frequency space domain learning. In *Proceedings of the AAAI Conference on Artificial Intelligence (AAAI)*, pages 5052–5060, 2024.
- [Thies *et al.*, 2016] Justus Thies, Michael Zollhofer, Marc Stamminger, Christian Theobalt, and Matthias Niessner. Face2face: Real-time face capture and reenactment of rgb videos. In *Proceedings of the IEEE Conference on Computer Vision and Pattern Recognition (CVPR)*, June 2016.
- [Thies *et al.*, 2019] Justus Thies, Michael Zollhöfer, and Matthias Nießner. Deferred neural rendering: Image synthesis using neural textures. *ACM Transactions on Graphics*, 38(4):1–12, 2019.
- [Tian *et al.*, 2024] Jiahe Tian, Cai Yu, Xi Wang, Peng Chen, Zihao Xiao, Jiao Dai, Jizhong Han, and Yesheng Chai. Real appearance modeling for more general deepfake detection. In *Proceedings of The 18th European Conference on Computer Vision (ECCV)*, pages 402–419, 2024.
- [Xu *et al.*, 2023] Yuting Xu, Jian Liang, Gengyun Jia, Ziming Yang, Yanhao Zhang, and Ran He. Tall: Thumbnail layout for deepfake video detection. In *Proceedings of the IEEE/CVF International Conference on Computer Vision (ICCV)*, pages 22658–22668, October 2023.
- [Xu *et al.*, 2024] Yuting Xu, Jian Liang, Lijun Sheng, and Xiao-Yu Zhang. Towards generalizable deepfake video detection with thumbnail layout and graph reasoning. *arXiv preprint arXiv:2403.10261*, 2024.
- [Yang *et al.*, 2023] Wenyuan Yang, Xiaoyu Zhou, Zhikai Chen, Bofei Guo, Zhongjie Ba, Zhihua Xia, Xiaochun Cao, and Kui Ren. Avoid-df: Audio-visual joint learning for detecting deepfake. *IEEE Transactions on Information Forensics and Security*, 18:2015–2029, 2023.
- [Zhang *et al.*, 2024] Daichi Zhang, Zihao Xiao, Shikun Li, Fanzhao Lin, Jianmin Li, and Shiming Ge. Learning natural consistency representation for face forgery video detection. In *Proceedings of The 18th European Conference on Computer Vision (ECCV)*, pages 407–424. Springer, 2024.
- [Zhao *et al.*, 2021] Tianchen Zhao, Xiang Xu, Mingze Xu, Hui Ding, Yuanjun Xiong, and Wei Xia. Learning self-consistency for deepfake detection. In *Proceedings of the IEEE/CVF International Conference on Computer Vision (ICCV)*, pages 15023–15033, 2021.
- [Zheng *et al.*, 2021] Yinglin Zheng, Jianmin Bao, Dong Chen, Ming Zeng, and Fang Wen. Exploring temporal coherence for more general video face forgery detection. In *Proceedings of the IEEE/CVF International Conference on Computer Vision (ICCV)*, pages 15044–15054, 2021.
- [Zhou *et al.*, 2021] Tianfei Zhou, Wenguan Wang, Zhiyuan Liang, and Jianbing Shen. Face forensics in the wild. In *Proceedings of the IEEE/CVF Conference on Computer Vision and Pattern Recognition (CVPR)*, pages 5778–5788, June 2021.
- [Zhu *et al.*, 2024] Lianghui Zhu, Bencheng Liao, Qian Zhang, Xinlong Wang, Wenyu Liu, and Xinggong Wang. Vision mamba: Efficient visual representation learning with bidirectional state space model. *arXiv preprint arXiv:2401.09417*, 2024.